


Nonlinear fluid damping models for hydraulic bushing under sinusoidal or transient excitation

Proc IMechE Part D:
J Automobile Engineering
1–10
© IMechE 2018
Reprints and permissions:
sagepub.co.uk/journalsPermissions.nav
DOI: 10.1177/0954407017751787
journals.sagepub.com/home/pid


Luke Fredette, Siddharth Rath and Rajendra Singh

Abstract

Hydraulic bushings are typically characterized in terms of sinusoidal dynamic stiffness at lower frequencies over a range of excitation amplitudes. However, in practice they are also exposed to severe transient loads in conjunction with sinusoidal excitations. Three improved nonlinear, lumped parameter models for hydraulic bushings are developed with the goal of concurrently predicting amplitude-sensitive dynamic responses to both sinusoidal and step-like excitations using a common dynamic model with the same parameters. First, a fluid resistance element is introduced which extends previous formulations by relaxing the assumption of fully developed turbulent flow, and capturing the transition from laminar flow to turbulence. Second, a bleed orifice element between the two compliance chambers is incorporated to simulate leakage observed in laboratory testing. The sensitivity of the dynamic responses to linearized model parameters is used to guide the parameter identification procedure. Measured dynamic stiffness spectra and step-like responses provide experimental validation of the proposed formulations. The new formulations achieve improved predictions of dynamic stiffness or force using exactly the same set of model parameters at several excitation amplitudes in both time and frequency domains.

Keywords

Damping characterization, dynamic simulation, hydraulic device, suspension bushings, vibration control

Date received: 15 March 2017; accepted: 17 November 2017

Introduction

Vibration isolators are typically characterized using frequency-domain dynamic stiffness based on non-resonant sinusoidal tests.^{1,2} In particular, hydraulic bushings exhibit substantial sensitivity to the nature and amplitude of dynamic loading.^{2–7} However, limited treatment is given in the literature or in practice to nonlinear design features that might cause or influence amplitude-dependent behavior, although several investigators have recently begun to address this topic.^{3–8} Gil-Negrete et al.³ examined the nonlinear behavior of elastomeric structural material in a finite element model of a hydraulic bushing. Arzanpour and Golnaraghi⁴ introduced a nonlinear model for an active compliance chamber into an otherwise linear hydraulic bushing model. He and Singh⁵ developed discontinuously nonlinear models for a hydraulic engine mount (similar to hydraulic bushings, but with different dynamic characteristics because of the decoupler and very compliant lower chamber). Their study found that the chamber compliances significantly varied with time under step

and realistic transient excitations; they did not, however, use the same model to examine the frequency-domain responses over a range of excitation amplitudes. Of particular interest, Chai et al.⁸ developed separate nonlinear models of hydraulic bushing concepts which were used to predict responses to steady-state sinusoidal or transient excitation profiles. These studies were undertaken on a laboratory device, and assumed fully developed turbulent flow in long inertia tracks as well as in short passages (such as the leakage paths). Fredette et al.^{6,7} developed an experimental procedure to measure and estimate the nonlinear fluid compliance of a

Department of Mechanical and Aerospace Engineering, Ohio State University, USA

Corresponding author:

Rajendra Singh, Department of Mechanical and Aerospace Engineering, Acoustics and Dynamics Laboratory, NSF Smart Vehicle Concepts Center, The Ohio State University, Columbus, Ohio 43210, USA.
Email: singh.3@osu.edu

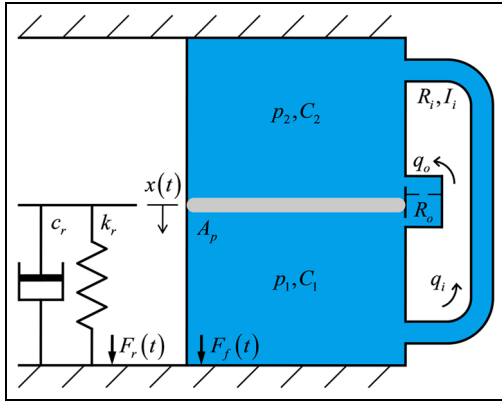


Figure 1. Lumped parameter model of the hydraulic bushing. Here, the spring constant (k_r) and damping coefficient (c_r) describe the behavior of the structural (rubber path) subsystem. The fluid system state includes the pressure in each chamber (p_1 , p_2) and the volumetric flow in the inertia track (q_i) and leakage paths (q_o). Additional model parameters include the effective pumping area of the inner sleeve (A_p), the fluid compliance of each fluid chamber (C_1 , C_2), the fluid inductance in the inertia track (I_i), and the fluid resistances of the inertia track and leakage paths (R_i and R_o , respectively).

production hydraulic bushing, which improved the amplitude dependent dynamic stiffness predictions in the frequency domain. However, amplitude dependent transient responses are yet to be properly studied. As such, the effects of nonlinear, time-varying model parameters on displacement amplitude sensitive responses in both the time and frequency domains must be better understood. Therefore, the goal of this paper is to introduce new nonlinear elements to better describe the amplitude sensitive dynamic behavior of a hydraulic bushing in response to steady-state harmonic or transient excitations. The intent here is to develop a common formulation (similar to those employed by Chai et al.⁸ or Fredette et al.^{6,7}) that would consistently work in both domains given the exact same dynamic system parameters, and thereby overcome the limitations of our prior work.⁸

Problem formulation

This article seeks to extend the recent article by Chai et al.⁸ by improving the damping formulations while including other relevant nonlinear elements^{6,7} into a single dynamic system model which is able to predict the dynamic response of a hydraulic bushing in both time and frequency domains with a unified set of parameters. The scope is limited to the development of minimal order, feature-based hydraulic bushing models which would predict amplitude-sensitive dynamic responses to both steady-state harmonic and step-like transient excitations. A production grade hydraulic bushing is used as the main example case for this study (unlike the laboratory device employed by Chai et al.⁸), with features depicted in the system model of Figure 1,

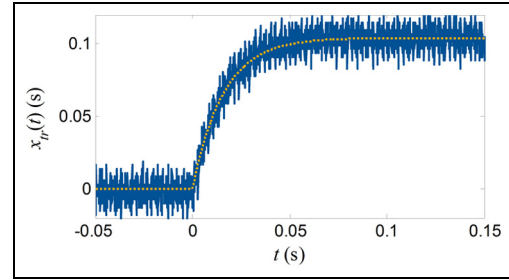


Figure 2. Small amplitude (0.1 mm) “step-like” displacement excitation profile that is generated by the non-resonant test machine. Key: — : measured; - - - curve-fit.

with relevant parameters. The device is excited by a dynamic displacement of the inner sleeve, $x(t)$, under a given mean load. The dynamic loads transmitted through the device to the rigid base are divided into two key load paths through the elastomeric structure (F_r) and through the fluid subsystem (F_f). The steady-state harmonic and transient excitation functions are chosen to coincide with the measured dynamic displacement profiles of an elastomeric test machine,⁹ and are respectively given as follows

$$x_{ss}(t) = \frac{x_a}{2} \sin(2\pi\Omega t) \quad (1)$$

$$x_{tr}(t) = x_a \left(1 - e^{-t/\tau}\right) \quad (2)$$

where Ω is the steady-state excitation frequency (in Hz), τ is the transient excitation time constant (a property of the test machine), and x_a is the excitation amplitude in terms of either peak-to-peak for sinusoidal input (equation (1)) or step height for transient input (equation (2)). Although sinusoidal testing of elastomeric devices is commonly employed, the “step-like” characterization is rare. A correlation between the theoretical (as given in equation (2)) and measured displacement signals is given in Figure 2 for a 0.1 mm step height. With this small excitation amplitude, a high-frequency dithering signal adds a substantial amount of noise to the displacement, so a low-pass filter is applied to the signal prior to curve-fitting. This effect is substantially reduced for larger excitation amplitudes, where the signal-to-noise ratio would be much higher.

For the sake of illustration, measured dynamic properties of the example hydraulic bushing are given in terms of dynamic stiffness magnitude (K_m), loss angle (ϕ_m), and transient responses in Figures 3 and 4, respectively, for three excitation amplitudes. Here, k_s is the static stiffness of the bushing. The scope is limited to uniaxial motion, component-level characterization at 0.1, 1.0, and 2.0 mm excitation amplitudes (in terms of peak-to-peak or step height) and a frequency range of up to 50 Hz (for the sinusoidal test). Specific objectives include: (1) developing a quasi-linear model (using the transfer function method in the Laplace domain) which should describe amplitude sensitivity essentially

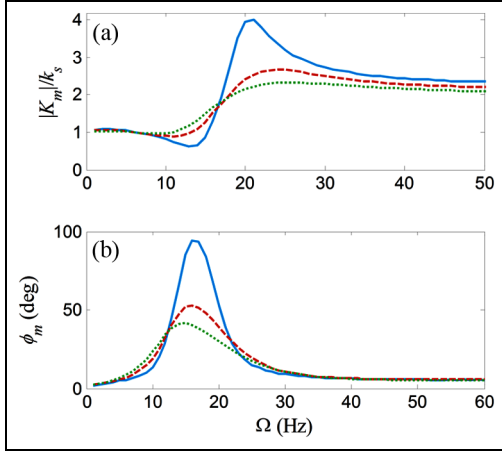


Figure 3. Effect of the sinusoidal excitation amplitude on the measured (a) stiffness magnitude and (b) loss angle. Key: —: 0.1 mm peak-to-peak; - - - 1.0 mm peak-to-peak; 2.0 mm peak-to-peak.

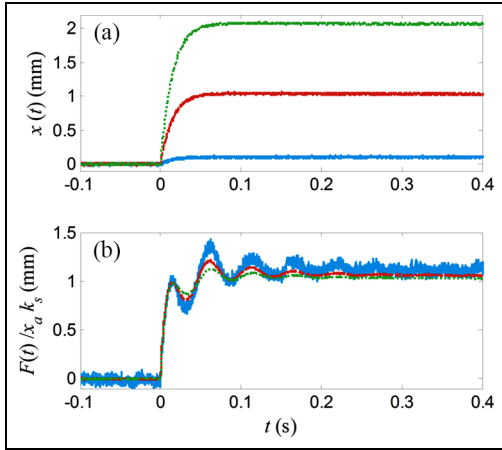


Figure 4. Effect of the step excitation amplitude on measured step responses of a hydraulic bushing. (a) “Step-like” excitation signals and (b) normalized transmitted force responses. Key: — 0.1 mm step height; - - - 1.0 mm step height; 2.0 mm step height.

in the frequency domain, and (2) development of two improved nonlinear fluid damping models to capture amplitude sensitive responses to both steady-state sinusoidal and transient, “step-like” displacement excitations. An overview of the models utilized or developed in this paper is given in Table 1. Figure 5 displays

frequency and time domain responses of the baseline⁷ (Model 0) which was recently developed, highlights the insufficiency of the damping characterization.

Quasi-linear model (I)

The quasi-linear modeling approach is based on an adaptation of the linear time-invariant system theory to capture amplitude sensitivity. Each parameter of the quasi-linear model assumes a value which may vary with the excitation amplitude. The governing equations of the linear system of Figure 1 are defined as

$$C_1 \dot{p}_1 = A_p \dot{x} - q_i - q_o \quad (3a)$$

$$C_2 \dot{p}_2 = -A_p \dot{x} + q_i + q_o \quad (3b)$$

$$I_i \dot{q}_i = p_1 - p_2 - R_i q_i \quad (3c)$$

$$p_1 - p_2 = R_o q_o \quad (3d)$$

$$F_f = A_p (p_1 - p_2) \quad (3e)$$

$$F_r = k_r x + c_r \dot{x} \quad (3f)$$

Taking the Laplace transform of these equations and consolidating gives the dynamic stiffness transfer function

$$K_I(s) = \frac{a_3 s^3 + a_2 s^2 + a_1 s + a_0}{s^2 + a_5 s + a_4} \quad (4)$$

where

$$a_0 = 2k_r \frac{R_i + R_o}{I_i R_o C} \quad (5a)$$

$$a_1 = k_r \left(\frac{R_i}{I_i} + \frac{2}{R_o C} \right) + 2c_r \frac{R_i + R_o}{I_i R_o C} + \frac{2A_p^2 R_i}{I_i C} \quad (5b)$$

$$a_2 = k_r + c_r \left(\frac{R_i}{I_i} + \frac{2}{R_o C} \right) + \frac{2A_p^2}{C} \quad (5c)$$

$$a_3 = c_r \quad (5d)$$

$$a_4 = \frac{R_i + R_o}{I_i R_o C} \quad (5e)$$

$$a_5 = \left(\frac{R_i}{I_i} + \frac{2}{R_o C} \right) \quad (5f)$$

Since this approach is very similar to the prior work,^{6,7} details of parameter estimation are not given here.

The dynamic stiffness spectra of Model I are compared with measurements in terms of magnitude and phase in Figure 6 for all three excitation amplitudes, showing good agreement. The quasi-linear model from

Table 1. Overview of nonlinear and quasi-linear models of hydraulic bushing.

Model	Type	Method or feature
0	NL	Baseline ⁷
I	QL	With curve-fit coefficients from dynamic stiffness measurement (in Laplace domain)
II	NL	Transitional flow in the inertia track
III	NL	Transitional flow in the inertia track and leakage path

NL: nonlinear; QL: quasi-linear.

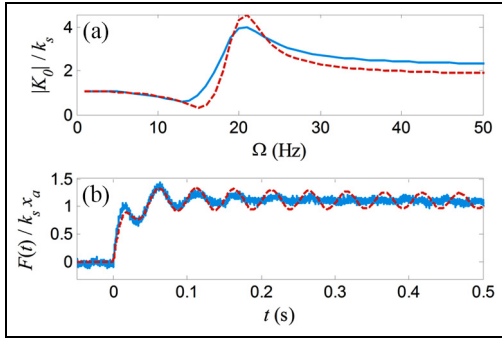


Figure 5. State of the art for nonlinear, lumped-parameter hydraulic bushing formulations (Model 0 as described in Table 1) in the (a) frequency and (b) time domains, showing moderate agreement with measurement. Note, in particular, that the formulation has insufficient fidelity to capture the decay of oscillations in the transient response. Key: — measurement; - - - model 0.

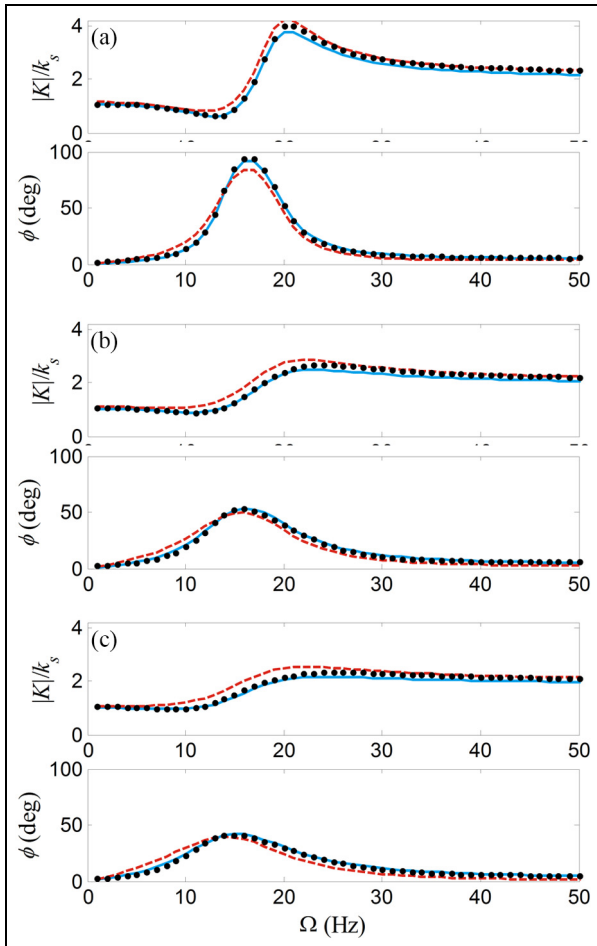


Figure 6. Results of the quasi-linear formulation (Model I) in terms of the dynamic stiffness magnitude and loss angle spectra when compared with measurements at multiple amplitudes: (a) 0.1 mm peak-to-peak; (b) 1.0 mm peak-to-peak; (c) 2.0 mm peak-to-peak. Key: — Model I; - - - Model I with $R_o \rightarrow \infty$; • measurement.

Fredette et al.⁷ (which is equivalent to model I as $R_o \rightarrow \infty$) is also compared. However, it may not be

Table 2. Quantification of error associated with the quasi-linear formulation (Model I) when compared with the dynamic stiffness measurement.

Excitation amplitude (mm)	RMS error, ε_I for Model I	RMS error for Model I when $R_o \rightarrow \infty$
0.1	0.0252	0.0469
1.0	0.0198	0.0394
2.0	0.0167	0.0478

RMS: root mean squared.

clear from the plot whether the inclusion of the R_o element provides any improvement. A root-mean-squared (RMS) error definition quantifies the error for this model, where k_s is the static stiffness,

$$\varepsilon_I = \frac{1}{Nk_s^2} \sum |\tilde{K}_I - \tilde{K}_m|^2 \quad (6)$$

Table 2 contains the RMS error of each model at all three amplitudes. Observe that the error of Model I is reduced with a finite value of R_o .

Although Model I captures the dynamic stiffness behavior of hydraulic bushings with relatively high accuracy (compared with measurements), its effectiveness is largely confined to the frequency domain. This is demonstrated by calculating the response of Model I to a step-like input. The excitation of equation (2) may be expressed in the Laplace domain

$$X_{tr}(s) = \frac{x_a}{s(\tau s + 1)} \quad (7)$$

yielding the following transmitted force

$$F_{tr}(t) = \mathcal{L}^{-1}\{K_I(s)X_{tr}(s)\} \quad (8)$$

where the inverse Laplace transform is defined as

$$\mathcal{L}^{-1}\{X(s)\} = \frac{1}{2\pi i} \int_{-i\infty}^{i\infty} e^{st} X(s) ds \quad (9)$$

as long as all singular points of $X(s)$ have negative real parts. For the sake of brevity, $F_{tr}(t)$ is plotted in Figure 7 rather than explicitly defining the analytical expression. It is immediately clear that Model I does not capture the salient physics of the hydraulic bushing under transient excitation.

Nonlinear fluid system elements

Nonlinear fluid compliance

The fluid compliance of the pumping chambers employs the nonlinear formulation used in the prior literature^{6,7} for this device

$$C(t) = \beta_2 p^2(t) + \beta_1 p(t) + \beta_0, \quad (10)$$

where $p(t)$ is the dynamic pressure in the chamber and the β coefficients are experimentally obtained. This

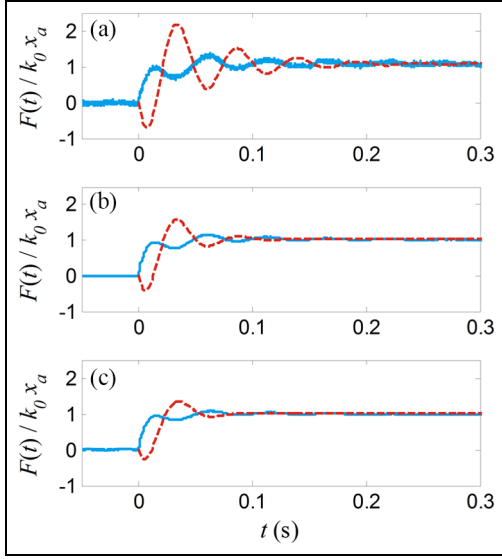


Figure 7. Time domain responses of quasi-linear formulation (Model I) to “step-like” excitations of multiple amplitudes: (a) 0.1 mm step height; (b) 1.0 mm step height; (c) 2.0 mm step height. Key: — measurement; - - - Model I.

element enhances the characterization of the structural-fluid interaction in the example, particularly given its sensitivity to the excitation amplitude.

Transitional flow in the inertia track (models II and III)

In the prior literature, characterization of the fluid resistance in the inertia track of a hydraulic bushing has assumed classical flow conditions, such as the fully developed laminar flow in a capillary tube^{1–5} or turbulent flow in a long duct.^{6–8} While these provide a baseline to approximate the flow condition in the inertia track of a hydraulic bushing, the combination of complex geometry and dynamic excitation suggest that an improved fluid resistance model would be necessary to adequately describe the physics of both the sinusoidal and transient excitations.

For a steady flow at low velocities in a long pipe (with $L \gg D$), Newtonian fluids tend to follow the well-known Hagen–Poiseuille law¹⁰

$$\Delta p(t) = \frac{128\mu L}{\pi D^4} q(t) \quad (11)$$

Where $\Delta p(t)$ is the dynamic pressure difference between the two fluid chambers, μ is the dynamic viscosity of the fluid, L and D are the length and hydraulic diameter of the pipe, respectively, and q is the dynamic volumetric flow rate. This formulation can be improved by the addition of another term which includes the losses due to sharp-edged entrance/exit effects, as well as the effect of accelerating fluid while the velocity profile is developing¹⁰

$$\Delta p(t) = \frac{128\mu L_i}{\pi D_i^4} \left(1 + 0.0434 \frac{D_i}{L_i} \mathcal{R}_i(t) \right) q_i(t) \quad (12)$$

where \mathcal{R}_i is the Reynolds number in the inertia track, ρ is the fluid density, and A is the pipe’s cross-sectional (hydraulic) area

$$\mathcal{R}_i(t) = \frac{\rho D_i |q_i(t)|}{\mu A_i} \quad (13)$$

When the Reynolds number increases beyond a certain threshold, \mathcal{R}_T , the flow condition transitions to turbulent flow. For a smooth pipe, this transition occurs around $\mathcal{R}_{i,T} = 2000 - 4000$, but this number may be lower for a rougher pipe wall or when the pipe geometry is more complex. The pressure drop due to the developed turbulent flow is given by¹⁰

$$\Delta p(t) = 0.242 \frac{\mu^{0.25} \rho^{0.75} L_i}{D_i^{4.75}} q_i^{1.75}(t) \quad (14)$$

for Reynolds numbers in excess of the transitional value.

Under dynamic excitation, the exact flow condition would be very difficult to ascertain, so approximations must be made using engineering assumptions. For dynamic flow which spans the laminar, transitional, and turbulent regimes, all regimes must be included in the model to improve fluid damping predictions. This is accomplished by using equation (10) for low Reynolds numbers, equation (12) for high Reynolds numbers, and a smoothed switching function near the transition. Pressure drop in the inertia track is defined by

$$\Delta p(t) = R_i(q_i(t)) q_i(t) \quad (15)$$

where $R_i(t)$ is the transitional, nonlinear fluid resistance:

$$R_i(t) = \frac{128\alpha_{i1}\mu L_i}{\pi D_i^4} \left(1 + 0.0434 \frac{D_i}{L_i} \mathcal{R}_i(t) \right) + \left(0.242\alpha_{i2} \frac{\mu^{0.25} \rho^{0.75} L_i}{D_i^{4.75}} |q_i(t)|^{0.75} - \frac{128\alpha_{i1}\mu L_i}{\pi D_i^4} \left(1 + 0.0434 \frac{D_i}{L_i} \mathcal{R}_i(t) \right) \right) u(|q_i(t)|, q_{i,T}, \sigma_i) \quad (16)$$

using the smooth switching function

$$u(q, q_T, \sigma) = \frac{1 + \tanh(\sigma(q - q_T))}{2} \quad (17)$$

Here, the α_i coefficients are the well-known correction factors to account for additional losses ($1 \leq \alpha_i \leq 1.5$) and σ_i is an empirical smoothing factor which controls the width of the transition region between the laminar and turbulent flow conditions. Figure 8 depicts the fluid resistance over a range of applicable Reynolds numbers in all three flow regimes.

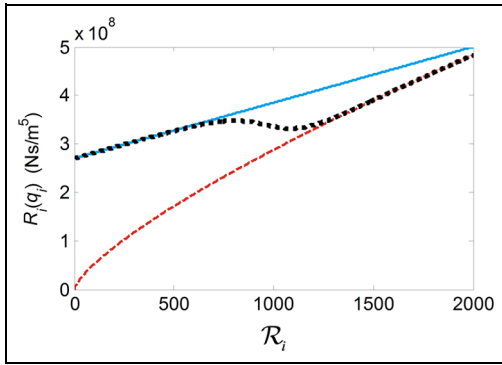


Figure 8. Illustration of proposed nonlinear fluid resistance model of the inertia track that captures laminar, transitional, and turbulent flow regimes. Here, \mathcal{R}_i is the Reynolds number. Key: — modified laminar flow formulation; - - - turbulent flow formulation; ■ ■ ■ transitional flow formulation.

Leakage path (model III)

Some hydraulic bushings have an intentional design feature which opens a bleed (or unintentional leakage) path between the two pumping chambers when a sufficiently large pressure differential builds up. This would allow fluid to bypass the tuned dynamics of the inertia track. In the example of hydraulic bushing used in this paper, a thin rubber wall separates the two chambers, and it may bend over and allow flow to pass by if the relative pressure difference between the chambers exceeds (say) 200 kPa quasi-statically. Under dynamic loading conditions, this value might be lower. Since the leakage path resembles a thin crack as the seal between the two chambers begins to fail, the leakage path is assumed to be a slit-like orifice of rectangular cross-section. The cross-sectional dimensions of this slit are assumed to be 300 times smaller than the inertia track to simulate the leakage path. Since this path is a very short, inertial effects are negligible. Kim and Singh¹¹ have experimentally and computationally examined the parallel leakage paths in hydraulic engine mounts and thus their significance in influencing the frequency domain properties is somewhat understood in the context of an engine mounting system.

The fluid resistance of the leakage path within the bushing, like that of the inertia track, depends on whether the flow regime is laminar, turbulent, or in the transition. The flow condition in the orifice (given by

subscript o) is determined by the value of the Reynolds number

$$\mathcal{R}_o(t) = \frac{\rho D_o |q_o(t)|}{\mu A_o} \quad (18)$$

where D_o is the hydraulic diameter of the leakage path, and A_o is its cross-sectional area. The transitional Reynolds number for an orifice is¹⁰

$$\mathcal{R}_{o,T} = \left(\frac{0.611}{\delta} \right)^2 \quad (19)$$

where δ is called the laminar flow coefficient; typically, $\delta = 0.16$ for a sharp-edged slit-like orifice. Figure 9 depicts the nature of the laminar and turbulent flow through an orifice. The pressure drop due to the laminar flow is given by

$$\Delta p(t) = \frac{\mu}{2\delta^2 D_o A_o} q_o(t) \quad (20)$$

while the pressure drop due to the turbulent flow is defined by

$$\Delta p(t) = \frac{\rho(\pi + 2)^2}{2\pi^2 A_o^2} q_o^2(t) \quad (21)$$

Combining these with the smoothed switching function (where σ_o is the transition smoothing coefficient for the leakage path), the fluid resistance for transitional flow in the leakage path is formulated as follows

$$R_o(t) = \frac{\mu}{2\delta^2 D_o A_o} + \left(\rho \frac{(\pi + 2)^2}{2\pi^2 A_o^2} |q_o(t)| - \frac{\mu}{2\delta^2 D_o A_o} \right) u(q_o(t), q_{o,T}, \sigma_o) \quad (22)$$

Figure 10 contains a plot of leakage path resistance versus Reynolds number, comparing laminar, turbulent, and transitional flow models.

Nonlinear simulation in time and frequency domains

The governing equations (3a, b, c, d, e) for the fluid subsystem of the hydraulic bushing are numerically integrated in the time domain using a Runge–Kutta

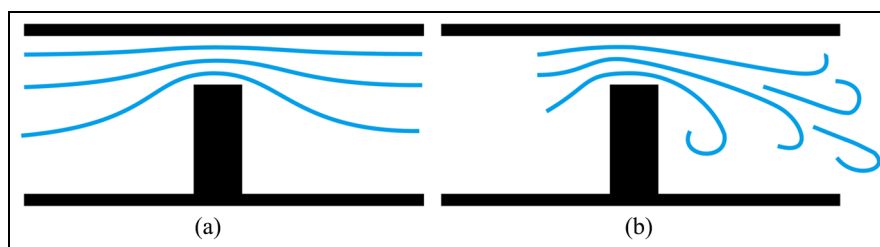


Figure 9. Qualitative representation of (a) laminar and (b) turbulent flow through the leakage path.

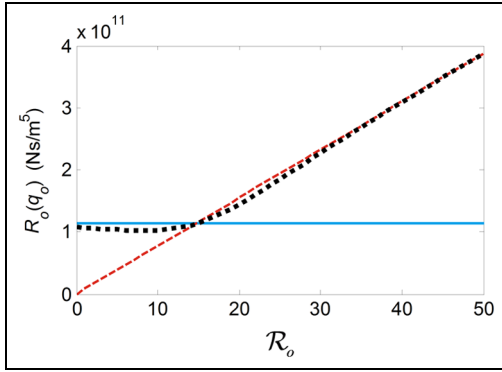


Figure 10. Proposed nonlinear fluid resistance model of the leakage path that captures laminar, transitional, and turbulent flow regimes. Key: — modified laminar flow formulation; - - - turbulent flow formulation; . . . transitional flow formulation.

solver in Matlab.¹² Model II modifies equation (3c) to include the transitional flow resistance model $R_i = R_i(q_i)$, and equation (3d) such that $R_o \rightarrow \infty$. Model III also includes the transitional flow in the leakage path. Accordingly, the effects of each nonlinear dissipative element may be studied as well as interactions among them.

Both the steady-state harmonic and transient (step response) simulations use the same equations, model parameters, and integration method. For the sinusoidal excitation, 40 periods are simulated at each frequency to allow the steady state to emerge. Then a sine wave (represented in the complex domain as $\tilde{F}_f(\Omega)$) is curve-fit to the integrated signal to remove any harmonic distortion from the nonlinear model. The forces transmitted through both paths are combined, and the complex-valued dynamic stiffness at any frequency is calculated

$$\tilde{K}(\Omega) = \frac{\tilde{F}_f(\Omega) + \tilde{F}_r(\Omega)}{x_a/2} \quad (23)$$

The final state after each frequency is used as the initial condition for the next frequency. This way, a true stepped frequency sweep over the desired bandwidth (in this case, up to 50 Hz) is simulated in an efficient manner. For the transient excitation, no post-processing is necessary, and thus the simulation outputs the transmitted force in the time domain as, $F(t) = F_r(t) + F_f(t)$.

The dynamic simulation results for Model III are compared with measurements and the results of prior lumped-parameter models (via Model 0) are shown in Figure 11 for both large and small amplitudes of excitation. Model III's improved damping characterization enhances dynamic predictions over the work reported previously⁷ in both the time and frequency domains, bringing a degree of consistency to the minimal order modeling approach. Furthermore, the new nonlinear model predicts dynamic responses over a

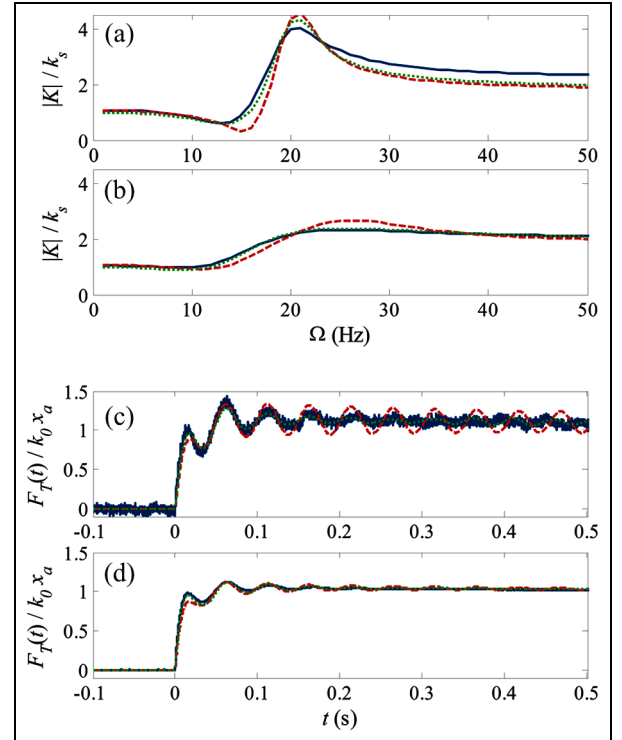


Figure 11. Improved simulation results for (a) 0.1 mm and (b) 2.0 mm peak-to-peak sinusoidal excitation in the frequency domain as well as (c) 0.1 mm and (d) 2.0 mm step excitation in the time domain. Model III is compared with the prior lumped-parameter models (Model 0) and measurements, showing a marked improvement in the damping characterization. Key: — measurement; - - - Model 0⁷; . . . Model III.

wide range of amplitudes, suggesting that the relevant physics have been well duplicated from the engineering design perspective.

Some physical insight may be gained into the functioning of a hydraulic bushing by examining the new nonlinear elements separately so as to rank-order their significance. For this example case, one particular nonlinearity tends to dominate the damping effects, as demonstrated by the comparison of Models 0, II, and III in Figure 12. Here, the aggregate effect of both the nonlinear elements (from inertia track and leakage paths) produces a response which is nearly identical to the model without a leakage path (Model II). This effect is consistent across both the time and frequency domains and at both high and low amplitudes. This does not imply, however, that the leakage path is negligible. Although the difference between Models II and III may be subtle, the leakage path has a significant effect on the amplitude dependence. Figure 13 shows the effect of adding a transitional flow based leakage path to Model 0. Although the introduction of a leakage path is ineffective at improving low-amplitude characterization, the high-amplitude predictions are nearly as accurate as Model III. This suggests that although the inertia track is the dominant nonlinearity (particularly at the lower amplitudes), an interaction

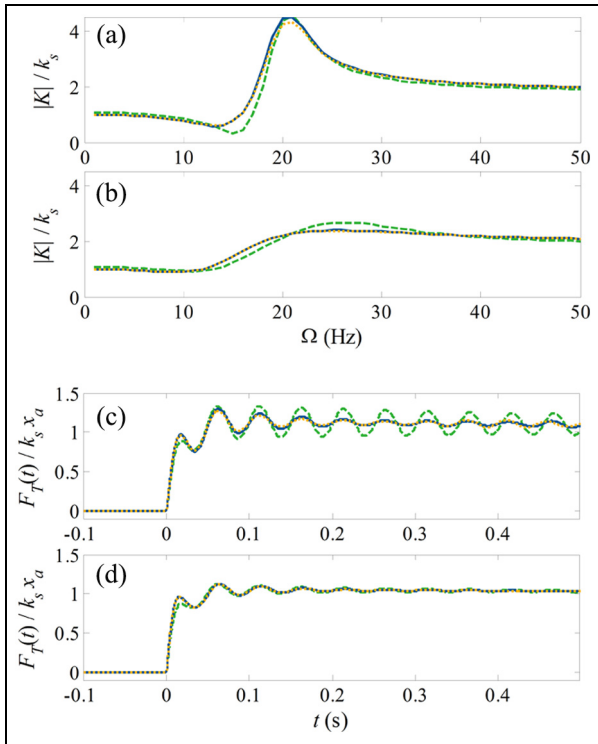


Figure 12. Comparison between the nonlinear models in terms of dynamic stiffness magnitude for (a) 0.1 mm and (b) 2.0 mm peak-to-peak excitation amplitudes and in terms of step response for (c) 0.1 mm and (d) 2.0 mm step height. Key: --- Model 0⁷; — Model II; -.-.- Model III.

exists between the nonlinear features of the device. Therefore, the leakage path should not be ignored.

Finally, Figure 14 displays the time varying nature of the fluid resistance of the inertia track $R_i(t)$ and leakage path $R_o(t)$ as they vary across an order of magnitude for a 2.0 mm excitation amplitude; however, both differ only by about a factor of two for a 0.1 mm excitation amplitude. It should be noted that in general, the values of $R_o(t)$ are approximately two orders of magnitude larger than $R_i(t)$. Much lower values of resistance cause more dynamic or oscillating flow to occur through the inertia track, offering a further reason why the inertia track resistance is the dominant nonlinear element.

Conclusion

Prediction of amplitude dependent dynamic behavior in hydraulic bushings requires significant due diligence, especially when both the frequency and time domain responses are of simultaneous interest. This is evident from certain sensitivities to response under the transient excitation which may be hidden (or just overlooked) in frequency domain studies. Capturing amplitude sensitive behavior for both steady-state sinusoidal and transient excitations requires in-depth characterization of not only the fluid compliance and inertia track

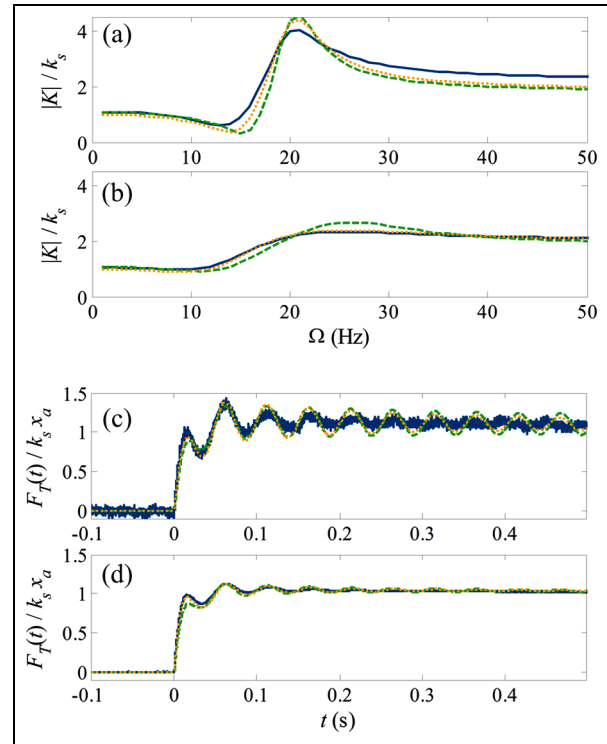


Figure 13. Result of introducing the nonlinear transitional flow resistance in the leakage path element in the absence of more dominant nonlinear features. This demonstrates a significant, amplitude-dependent effect in terms of both dynamic stiffness magnitude at (a) 0.1 mm and (b) 2.0 mm peak-to-peak excitation amplitudes and transient response for (c) 0.1 mm and (d) 2.0 mm step amplitudes. Key: — measurement; --- baseline Model 0⁷; -.-.- Model 0 with new transitional flow leakage path.

properties, but also their resistance characteristics. This paper investigated two dissipative mechanisms in a hydraulic bushing, and proposed a new or improved fluid resistance model based on laminar, turbulent, and transitional flow in both the inertia track and a leakage path between the two pumping chambers. A relatively high degree of accuracy is achieved by a nonlinear, lumped parameter model which includes both of these damping mechanisms, and improved insights are obtained. Although the inertia track resistance remains the dominant damping feature in hydraulic bushings, the leakage path is found to contribute to the damping as well, particularly at the higher amplitudes. Similar nonlinear analysis could be extended to other hydraulic devices (such as engine or vehicle body mounts¹³ and shock absorbers¹⁴) whose properties would depend on instantaneous or oscillating flow conditions. Finally, this article adds to the body of literature on hydraulic bushing models^{1-4,6-8} and in particular extends the recent work of Chai et al.⁸ Since minimal attention is given to the role played by rubber path damping in these publications (including this article), future work should be directed towards giving a careful examination of the elastomer characteristics.

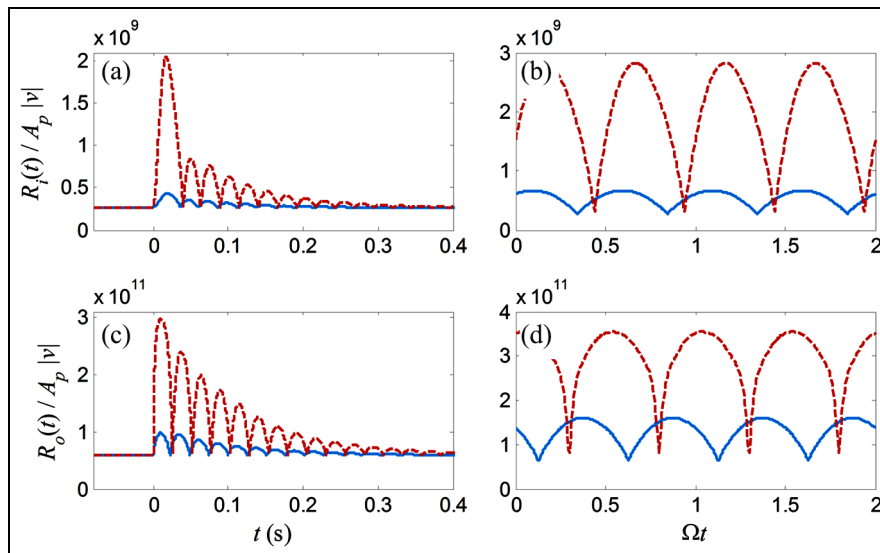


Figure 14. Time varying, nonlinear, transitional flow fluid resistance in the inertia track under (a) transient step and (b) steady-state sinusoidal excitation and in the leakage path under (c) step and (d) sinusoidal excitation. Key: — 0.1 mm excitation amplitude (peak-to-peak or step height); - - - 2.0 mm excitation amplitude.

Declaration of conflicting interests

The author(s) declared no potential conflicts of interest with respect to the research, authorship, and/or publication of this article.

Funding

The author(s) disclosed receipt of the following financial support for the research, authorship, and/or publication of this article: The authors would like to thank the member organizations of the Smart Vehicles Concepts Center (www.SmartVehicleCenter.org) such as Transportation Research Center, Inc., Honda R&D, F.tech, Ford Motor Company, and Tenneco, Inc. as well as the National Science Foundation Industry/University Cooperative Research Centers program (www.nsf.gov/iip/iucrc) for supporting this work. The Ohio State University's RIYA program (mae.osu.edu/riya) is also acknowledged for facilitating the internship for the second author.

References

1. Sauer W and Guy Y. Hydro bushings: innovative NVH solutions in chassis technology. SAE paper 2003-01-1475, 2003.
2. Chai T, Dreyer JT and Singh R. Frequency domain properties of hydraulic bushing with long and short passages: system identification using theory and experiment. *Mech Syst Signal Process* 2015; 56: 92–108.
3. Gil-Negrete N, Rivas A and Vinolas J. Predicting the dynamic behaviour of hydrobushings. *Shock Vibr* 2005; 12: 91–107.
4. Arzanpour S and Golnaraghi M. A novel semi-active magnetorheological bushing design for variable displacement engines. *J Intell Mater Syst Struct* 2008; 19: 989–1003.
5. He S and Singh R. Discontinuous compliance nonlinearities in the hydraulic engine mount. *J Sound Vibr* 2007; 307: 545–563.
6. Fredette L, Dreyer JT and Singh R. Dynamic analysis of hydraulic bushings with measured nonlinear compliance parameters. *SAE Int J Passeng Cars Mech Syst* 2015; 8: 1128–1136.
7. Fredette L, Dreyer JT, Rook TE, et al. Harmonic amplitude dependent dynamic stiffness of hydraulic bushings: alternate nonlinear models and experimental validation. *Mech Syst Signal Process* 2017; 75: 589–606.
8. Chai T, Dreyer JT and Singh R. Nonlinear dynamic properties of hydraulic suspension bushing with emphasis on the flow passage characteristics. *Proc IMechE Part D: J Automobile Engineering* 2015; 229: 1327–1344.
9. MTS. Elastomer test systems, Model 831.50 × 1000 Hz elastomer test system features high frequency test capability, https://mts.com/ucm/groups/public/documents/library/dev_002249.pdf (2004).
10. Merritt H. *Hydraulic control systems*. New York: John Wiley & Sons, 1967, 358 pp.
11. Kim G and Singh R. Nonlinear analysis of automotive hydraulic engine mount. *ASME J Dyn Syst Meas Control* 1993; 115: 482–487.
12. *MATLAB Release 2013b*. Natick, Massachusetts: The MathWorks, Inc.
13. Yu Y, Naganathan NG and Dukkipati RV. A literature review of automotive vehicle engine mounting systems. *Mech Mach Theory* 2001; 36: 123–142.
14. Duym S, Stiens R and Reybrouck K. Evaluation of shock absorber models. *Vehicle Syst Dyn* 1997; 27: 109–127.

Appendix I

Notation

$0, I, II, III$	model designations
A_p	effective pumping (force) area
a	transfer function coefficient

C	fluid compliance
c	viscous damping coefficient
D	hydraulic diameter
F	transmitted force
K	dynamic stiffness
k	static stiffness
I	fluid inertance
\mathcal{L}	Laplace transform
L	length of fluid passage
N	number of points
p	pressure
q	volumetric flow rate
R	fluid resistance
\mathcal{R}	Reynolds number
s	Laplace domain variable
t	time
u	smoothened step function
X	Laplace transform of displacement
x	displacement of inner sleeve
α, β	empirical parameters
δ	laminar flow coefficient
ε	error

μ	dynamic viscosity
ρ	fluid density
τ	time constant
Ω	excitation frequency (Hz)

Subscripts

a	amplitude (peak-to-peak or step height)
f	fluid path
i	inertia track
m	measured
o	leakage path
r	rubber path
s	static
T	laminar-turbulent transition
tr	transient excitation

Abbreviation

RMS	root mean squared
-----	-------------------